FULL PAPER

Controlling the Self-Assembly of Periodic Defect Patterns in Smectic Liquid Crystal Films with Electric Fields

*Iryna Gryn, Emmanuelle Lacaze, Roberto Bartolino, and Bruno Zappone**

Large-area periodic defect patterns are produced in smectic A liquid crystals confined between rigid plate electrodes that impose conflicting parallel and normal anchoring conditions, inducing the formation of topological defects. Highly oriented stripe patterns are created in samples thinner than 2 μm due to self-assembly of linear defect domains with period smaller than 4 μm, whereas hexagonal lattices of focal conic domains appear for thicker samples. The pattern type (1d/2d) and period can be controlled at the nematic–smectic phase transition by applying an electric field, which confines the defect domains to a thin surface layer with thickness comparable to the nematic coherence length. The pattern morphology persists in the smectic phase even after varying the field or switching it off. Bistable, non-equilibrium patterns are stabilized by topological constraints of the smectic phase that hinder the rearrangement of defects in response to field variations.

1. Introduction

Periodic soft materials with spontaneous breaking of translation symmetry such as block copolymers (lamellar, cylindrical, cubic and gyroid phases)[1–3] and liquid crystals (smectic, cholesteric and columnar phases)[4–10] are being actively investigated for creating self-assembled ordered structures and templates for micro and nanoscale applications. Periodic soft materials may help overcome the limits of current microfabrication techniques in terms of easiness, rapidity, cost and spatial resolution, with the added benefit of a large response to external stimuli.[11] In the past few years, thermotropic smectic A (SmA) liquid crystals (LC) have emerged as a promising class of materials for creating large-area 1d[12–15] and 2d[16–22] periodic micropatterns to be used in applications such as guided assembly of dispersed colloids and nanoparticles,[14,15,20,23] soft lithography[24,25] and microlens arrays.[26] SmA LCs are made of rod-like molecules that tend to align with each other along a common director, **n**, and form periodically spaced lamellae (layers) perpendicular to **n**, with period (layer thickness) a of the order of a few nm.[27] Since bending a lamella requires much less energy per unit area than changing its thickness, the shape of a curved lamella propagates to neighboring lamellae with negligible variation of the period a. This can be accomplished by shifting constant distances along the lamella normals, thereby generating a set of confocal surfaces with shared centers of curvature.[28–30] The orientation and shape of the confocal lamellae result from the balance between bulk elastic (structural) forces due to layer deformations, surface interactions imposing preferential orientations to **n** (anchoring), external electromagnetic fields and geometrical boundary conditions. In SmA films and periodic materials, the formation of patterns and their response to external fields are intimately connected to the nucleation, annihilation and rearrangement of topological defects.[28] In SmA films subject to conflicting anchoring conditions at opposite interfaces, the **n** field is distorted and the lamellae bend to satisfy both anchoring conditions. The deformation field is associated with singularities – disclination and dislocation lines, and wall defects – and may be partially released by allowing local departures from the anchoring conditions[21] and/or confocality rule.[29,31,32] Defects interact with each other and with the interfaces via long-range elastic forces and self-assemble into multi-defect domains whose symmetry reflects that of the interfaces. Surface interactions that do not impose any particular in-plane alignment, such as degenerate parallel (planar) and normal (homeotropic) anchoring, produce axially symmetric defect domains known as toroidal focal conic domains (FCDs) that self-organize into close-packed hexagonal lattices.[16–18,25] On the other hand, oriented 1d arrays of straight linear domains (LDs)[12–15,33] and lattices of eccentric FCDs[19,21] are created at the interface between air, inducing homeotropic anchoring, and a substrate inducing unidirectional planar anchoring.

In the present work, we considered homeotropic and unidirectional planar anchoring conditions for SmA films sandwiched between rigid electrode plates. An electric field was applied normal to the plates and the director **n** tended to align parallel to the field. We were able to create highly oriented 1d arrays and 2d lattices and control the pattern type (1d/2d) and period by varying the film thickness and/or the applied electric field. Striped patterns were stable over the entire temperature

I. Gryn
Dipartimento di Fisica
Università della Calabria
Via P. Bucci, 31/C, Arcavacata di Rende 87100, Italy
Dr. E. Lacaze
CNRS, UMR7588, Institut des
Nano-Sciences de Paris (INSP)
4 place Jussieu 75005, Paris, France
Prof. R. Bartolino, Dr. B. Zappone
CNR-IPCF and Liquid Crystal Laboratory
Via P. Bucci 31/C, Arcavacata di Rende 87100, Italy
E-mail: bruno.zappone@cnr.it

DOI: 10.1002/adfm.201402875

range of the SmA phase, as opposed to transitional effects reported in Cladis and Torza.[34] In contrast with field-driven electro-hydrodynamic patterns observed in the nematic (N) phase (Williams domains[27]), our patterns could be created with DC fields and corresponded to static arrangements of the SmA lamellae. Pattern morphology could be controlled at the N → SmA transition but remained largely unaffected by field variations applied in the SmA phase. Therefore, the system was bistable in the SmA phase, i.e., different pattern morphologies could be obtained for a same voltage depending on the voltage applied during the N-SmA transition. Such behavior indicates that large energy barriers hinder the rearrangement of defect patterns in response to applied fields.

2. Results

2.1. Field-Off Patterns

Figure 1 shows large-area periodic arrays of LDs obtained in the SmA phase of two thermotropic LCs, 8CB and SCE12, with different phase sequences (including chiral phases for SCE12) and chemical-physical properties. The samples were confined to a thickness $h \leq 7$ μm between glass plates treated to impose incompatible unidirectional planar anchoring (rubbed polymer polyimide, PI) and homeotropic anchoring (monolayer of silane surfactant, OTS).[35] Under a polarizing optical microscope (POM) with crossed polarizers, the samples appeared as a sequence of alternating dark (non-birefringent) and bright straight lines, perpendicular to the planar anchoring direction *x*. The transmitted light intensity showed a sinusoidal modulation along *x* due to a periodic variation of the refractive index. Such modulation diffracted the light of a green laser beam under normal incidence (Figure 1, inset).

When the sample thickness *h* increased above 1.3 μm, LD arrays coexisted with isolated FCDs and patches of a FCD lattice, which developed into a full close-packed 2d lattice as the thickness was increased above 2.2 μm (**Figure 2**).

Laser diffraction showed that the lattice was hexagonal (Figure 2, Inset). For both LD arrays and FCD lattices, the period *d* (lateral domain size) increased almost linearly when *h* increased, $d \approx d_0 + \alpha h$, with different slopes α and offset d_0 for LDs and FCDs (**Figure 3**). Notice that the slope was $\alpha = 2$ for LDs formed in both 8CB and SCE12, indicating that the same array structure was created by the two compounds, despite their different chemical structure. At the transition between the two pattern types, the lateral size of isolated FCD and the period of FCD patches were comparable to the period in LD regions.

In cells with uniform thickness *h*, the period *d* of LD arrays was constant. Uniform arrays covering areas as large as 0.1 mm^2 (more than 0.3 mm lateral size) could be routinely obtained. Also, LDs running across the entire uniform area without interruptions or changes in brightness were frequently observed (Figure 1). For a given *h*, the lateral size *d* varied slightly among the different domains and from sample to sample. The dispersion was $\delta d/d < 0.2$ for LD arrays and increased for FCD

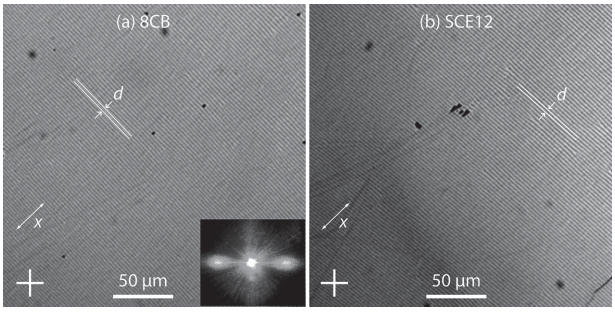

Figure 1. POM images of large-area, self-assembled arrays of LDs obtained in the absence of electric field. The planar anchoring direction was parallel to *x* and the polarizers were oriented as shown by the cross. a) 8CB sample with a thickness $h = 1.2$ μm and period $d = 2.6$ μm. Inset: Diffraction pattern for green laser light. b) SCE12 sample with $h = 1.2$ μm and period $d = 2.7$ μm.

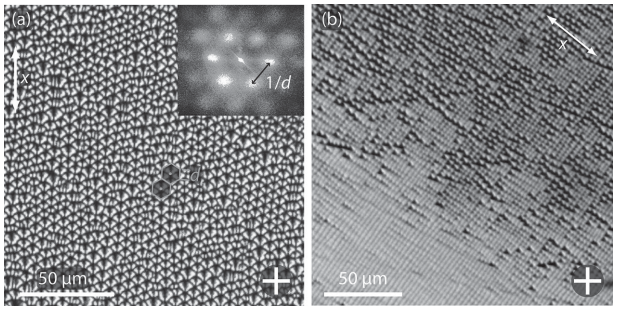

Figure 2. a) POM image of a close-packed lattice of non-toroidal FCDs obtained in the absence of electric field. The planar anchoring was parallel to *x* and the polarizers were oriented as shown by the cross. The sample thickness was $h = 2.7$ μm and the period $d = 4.6$ μm. Inset: Diffraction pattern at normal incidence for a green laser light, showing hexagonal symmetry. b) Region of coexistence at the transition between FCDs and LDs ($h = 1.2 - 1.8$ μm)

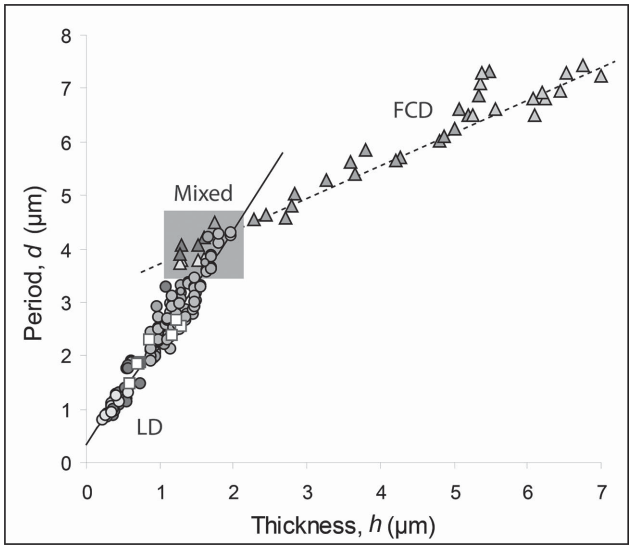

Figure 3. Lateral domain size (period) *d* as a function of the film thickness *h*. Circles and triangles indicate respectively LDs and FCDs for 8CB samples. White squares in the foreground correspond to LDs formed in SCE12. Solid and dotted lines are linear fits, $d = d_0 + \alpha h$, with $d_0 = 0.3$ μm and $\alpha = 2$ for LDs, and $d_0 = 3.1$ μm and $\alpha = 0.62$ for FCDs. Each color corresponds to a different sample.

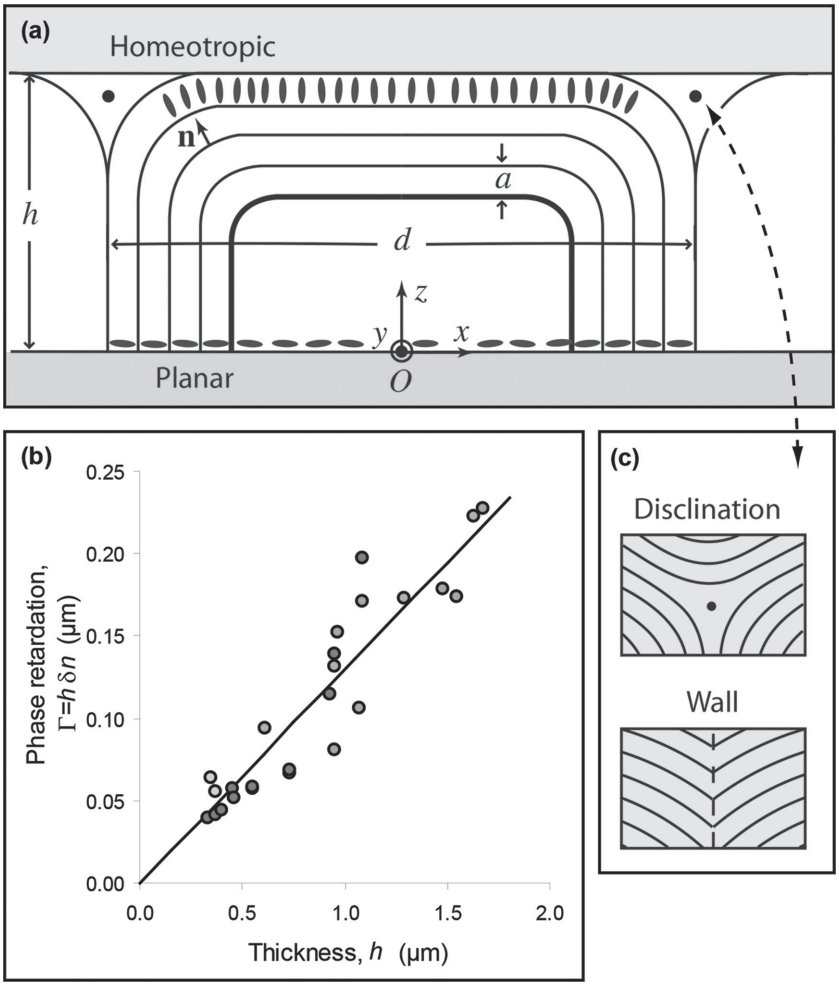

Figure 4. a) Cross-sectional view of the internal LD structure in the absence of a field. Molecules are shown as blue rods, lamellae as lines. **n** is the director, perpendicular to the lamellae, and *a* is the lamella thickness. Lamellae are added confocally to the lamella shown as a thick line. b) Phase retardation Γ of the brightest regions ($x = \pm d/2$) as a function of the sample thickness *h*. Different colors correspond to different samples. The solid line corresponds to $\Gamma = h\delta n$ with birefringence $\delta n = 0.13$. c) Disclination lines and curvature walls (black dots) are expected at the boundary between neighboring domains and at the domain center *O*.

lattices. Such dispersion is much larger than the experimental errors on *d*, and appears to be intrinsic to the mechanisms of defect nucleation and close-packed self-assembly that leads to pattern formation.

Simple POM observations of 8CB samples provided a coarse-grained picture of the director field inside the striped LD arrays presented in **Figure 4**a.

The director **n** lied in a vertical plane parallel to *x*, was invariant along the perpendicular direction *y* and was periodically tilted from the surface normal *z* towards the direction *x*. Because of the tilt modulation, laser diffraction was barely detectable when the light polarization was parallel to *y*, i.e., perpendicular to **n** and insensitive to the tilt modulation. Non-birefringent dark lines of the LD array corresponded to homeotropic regions where **n** was normal to the surfaces (zero tilt) across the film thickness, whereas bright lines corresponded to maximum tilt. In the bright lines, the optical phase retardation $\Gamma = h\delta n$ increased linearly with the sample thickness *h*, with local birefringence $\delta n = 0.13$ close to the maximum value $\delta n_0 = 0.165$ for 8CB at room temperature[36] (Figure 4b). This showed that **n** was planar (90° tilt) across most of the film thickness. Such coarse grained picture of the director field and lamellae arrangement in the LD arrays is similar to that obtained by POM for open 8CB films deposited on crystalline surfaces and further detailed by high-resolution X-ray diffraction measurements.[12,31,33,37] These studies have shown that LDs contain lamellae that satisfy both anchoring conditions by starting and ending with a vertical orientation (**n** planar) on the planar anchoring surface, and pass trough a horizontal orientation (**n** homeotropic) in between (see thick lamella in Figure 4a). The lamellae are shaped as hemicylinders flattened along the confinement direction *z*. Building on these ideas, we propose a simple explanation for the slope $\alpha = 2$ of the *d* vs *h* curve of LD arrays (Figure 3). When *h* increases, LDs grow confocally by propagating the flattened hemicylinder shape: adding one lamella on top increases the domain height *h* by *a* and the lateral size *d* by 2*a* (Figure 4a). However, when the domain has height *h* above the rubbed polymer substrate at the domain center ($x = 0$, Figure 4a), there should be $n = h/a$ lamellae inside it, spanning a distance $d = 2\,na = 2\,h$ along *x*. The presence of an offset such that $d = d_0 + 2\,h > 2\,h$ indicates that not all the lamellae inside of a LD are built confocally and there are non-confocal regions inside and surrounding the confocal domain. These regions are typically located in the proximity of topological defects. In our samples we expect a defect, most likely a disclination line, at the domain center where the confocal construction leaves the lamellae orientation undefined (point *O* with $x = 0$ and $z = 0$ in Figure 4a). At the domain boundary, the lamellae close to the homeotropic surface must be flat to conform to the boundary plate and suddenly bend by 90° to reach the polymer surface with a vertical orientation (point with $x = \pm d/2$ and $z = h$ in Figure 4a). Most likely, these lamellae locally violate the homeotropic anchoring and reach the domain boundary with a tilted orientation, thereby creating a curvature wall or a disclination line (Figure 4c).

It is more difficult to determine the lamellae arrangement inside the FCDs due their 3d nature implying many parameters to describe eccentricity, orientation, completeness, etc. By analogy with similar patterns obtained in open films[21] and closed cells[19,38] we deduce that the FCDs (Figure 2a) were non-toroidal (eccentric), with the major axis of the ellipse oriented along the anchoring direction *x* and the conjugated hyperbola lying in the vertical plane parallel to *x*.

2.2. Field-on Patterns

We prepared 8CB samples with thickness h = 6 – 12 μm that produce 2d lattices of FCDs in the absence of a field. When a DC voltage V was applied while keeping the samples in the SmA phase, the overall pattern morphology remained unaffected. However, when the samples were cooled down from the isotropic phase while applying the same voltage V, 1d arrays of LDs could be created at the N – SmA transition if V was sufficiently high (**Figure 5**).

The size d of the LDs increased approximately linearly with the film thickness h and decreased with V (**Figure 6**a). For V > 10 V, the period of the LDs was too small to be resolved by POM but the white light coming from the microscope lamp was diffracted along the x direction with a green-blue tint, indicative of a LD arrays with small period d. The slope of the d vs h line decreased as V increased and was smaller than the value α = 2 measured for LDs in the absence of a field. When V was decreased below about 5 V, FCDs appeared first in thick regions of the SmA sample, then in regions with decreasing thickness as V was further decreased. As for the E = 0 case (Figure 3), LDs coexisted with FCDs in the transition region.

This seemingly complex response to changes of thickness and voltage was much simplified by considering d as function of the inverse of the electric field $1/E = h/V$ (Figure 6b). All $d(h,V)$ curves reduced to a linear master curve, $d = d_0 + \alpha/E$, with slope α = 1.4 V and offset d_0 = 0.3 μm. Moreover, it became apparent that LDs and FCDs coexisted when $1/E$ was between 1.6 μm/V and 2.3 μm/V, and the transition from 2d to 1d was complete only for $1/E$ < 1/1.6 μm/V corresponding to E > 0.6 V/μm (Figure 6b). A similar behavior was observed when the field was modulated (AC voltage) at frequencies ranging from 0.1 to 100 kHz. For a given voltage V, the period of the LD arrays was uniform over areas with uniform thickness h (i.e., uniform E) and we could routinely obtain areas as wide as 0.3 mm showing uniform period d. The period dispersion was $\delta d / d$ < 0.2, comparable to that obtained for field-off patterns (Figure 1). In contrast to the latter case, the LDs were frequently interrupted and showed variations of brightness along their length (Figure 5). The average length of the uninterrupted domains was significantly smaller than the lateral extension of the uniform regions.

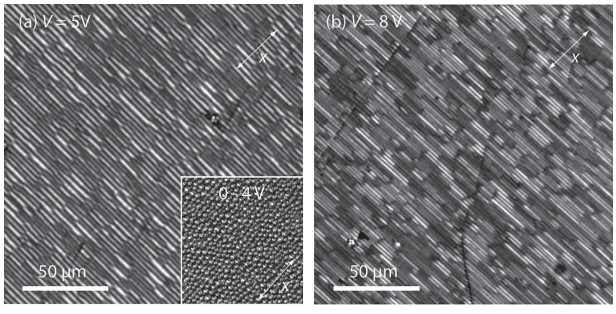

Figure 5. Arrays of LDs created by applying an electric field in an 8CB sample while cooling from the N to the SmA phase. a) Film thickness h = 7.1 μm, voltage V = 5 V. The inset shows the FCD lattice formed in the same region after cooling from N phase with a lower voltage. b) h = 8.1 μm, voltage V = 8 V.

To understand the similarities observed in the E = 0 case for a varying thickness and in the E > 0 case for a varying field strength, we consider the director field **n** in the N phase and how it changes in response to variation of E at the SmA-N transition (**Figure 7**).

The application of a field introduces a dielectric term: $(\varepsilon_a/2)$ $(\mathbf{n}\cdot\mathbf{E})^2$ in the free energy, where ε_a is the dielectric anisotropy, that couples the director distortion with the external field. When E is increased in the N phase, an increasingly thick portion of the LC film close to the surface inducing homeotropic anchoring becomes uniform and homeotropic (i.e., $\mathbf{n}\|\mathbf{E}$). The region where **n** significantly tilts from z and E becomes increasingly confined near the surface inducing planar anchoring. The thickness of this region is given by the electric coherence length $\xi = (K/\varepsilon_0\varepsilon_a)^{1/2}/E$, where K is the elastic constant of the LC and ε_0 the permittivity of vacuum.[27] For 8CB, K = 9 pN, ε_a = 9 and $\xi \approx 0.3$ μm/E at the N-SmA transition.[39] As the sample is cooled to the SmA phase, the homeotropic region turns into a set of mostly flat horizontal lamellae while curved lamellae are formed in the tilt region (Figures 7c and d). Thus the electric field E has an effect analogous to that of a compression that reduces – from h to ξ – the thickness available for creating curved lamellae. Accordingly, we can induce a transition from 1d arrays to 2d lattices either by decreasing the thickness with E = 0, or by increasing E. Following the model of Figure 4a and replacing h with ξ, we expect $d = d_0 + 2\ \xi = d_0 + 0.6\ /E$. While the offset was indeed d_0 = 0.3 μm, the size was found to increase with ξ faster than expected, $d = d_0 + 1.4\ /\ E = d_0 + 4.7\ \xi$, suggesting that the effective confinement thickness was larger than ξ. Clearly, the scaling argument relating d and E through ξ cannot be pushed further without considering the fine details of the **n** field distortion in the N phase and how **n** is reconfigured at the N-SmA transition to fulfill the additional constraint of constant layer thickness.

In a hybrid (planar-homeotropic) nematic cell subject to DC voltage, flexo-electricity and surface interactions (e.g., accumulation of ionic impurities at the electrodes) may create a polarization field **P** that contributes to the free energy with terms of the form $\mathbf{P}\cdot\mathbf{E}$.[40,41] These effects can be time-averaged to zero by applying AC fields with frequencies in the kHz range.[42] We obtained similar patterns for DC and AC fields (Figure 6b), showing that polarization effects in the N phase were secondary in establishing the properties of the patterns in the SmA phase. On the other hand, the additional constraints of the SmA phase on the **n** field may play an important role. For instance, for E > 0 the topmost layer (reaching the maximum height z) of a flattened hemicylinder does not reach the homeotropic boundary and does not have to conform to the rigid plate geometry. Therefore hemicylinders can be more rounded at the top and defects at the domain boundaries may differ from the E = 0 case (Figure 7c and 7d). These differences are also reflected in the behavior of the 1d-2d transition. For E = 0 (Figure 2b and 3), LDs and FCDs of comparable size d = 3.6 – 4.4 μm coexisted in the transition region (h = 1.3 – 1.9 μm). For E > 0 (Figure 6b), the domain size increased discontinuously at the transition, the FCD size being almost double the LD size. The size of the LDs and FCDs in the transition region were respectively smaller and larger than the size observed in the absence of a field.

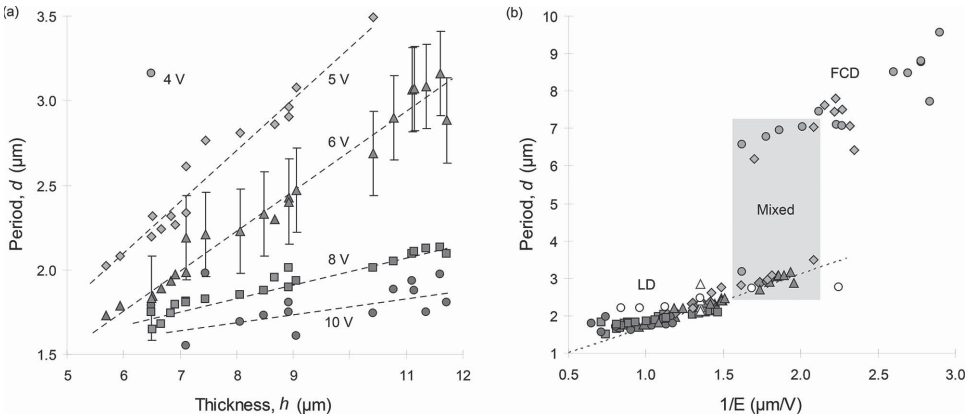

Figure 6. a) Lateral size d of LDs as a function of the film thickness h for different values of DC voltage V. One symbol is used for each voltage. For a given voltage, different colors correspond to different samples. For each V, the point with maximum d is the latest stable point before the transition to a FCD lattice. The error bar shows the typical dispersion of the d measurements. b) Size d as a function of the inverse of the electric field $E = V/h$. In the shaded region, LDs coexist with FCDs. The straight dotted line has equation $d = d_0 + \alpha/E$ with $d_0 = 0.3$ μm and $\alpha = 1.4$. White circles and triangles in the foreground correspond to sinusoidal AC fields with variable peak-to-peak amplitude E and fixed 1 kHz frequency, and variable frequency (0.1–100 kHz) with fixed amplitude, respectively.

2.3. Texture Persistence and Bistability

When the field was varied in the SmA phase after creating a 1d array or 2d lattice, the pattern type did not change and the period remained almost constant for more than one day after varying the field (**Figure 8**). For both LD arrays and FCD lattices we observed only a small decrease of domain birefringence due to widening of the homeotropic regions and/or decreasing birefringence of the bright regions. In particular, applying a field $E > 0.6$ V/μm during the N-SmA transition created a LD array, but switching from zero to the same value of E in the SmA phase did not replace the FCD lattice with a LD array. Therefore, the system was bistable and the creation of a 1d or 2d texture depended on how the field and temperature were varied to reach a particular state in the SmA phase.

When a FCD lattice was heated to the N phase without changing the field, a faint lattice texture was observed by POM in the N phase due to surface memory effect, i.e., the persistence in the N phase of the **n** field created on the substrates in the SmA phase.[21,43] The print could be erased in the isotropic phase by increasing the field voltage, and LD arrays could be created upon cooling into the SmA phase with $E > 0.6$ μm/V. However, when a LD array was heated to the N phase without changing the field, we could not detect the print of the LD texture. Therefore, surface memory effect may stabilize 2d pattern and hinder the field-induced transition to 1d array, but does not

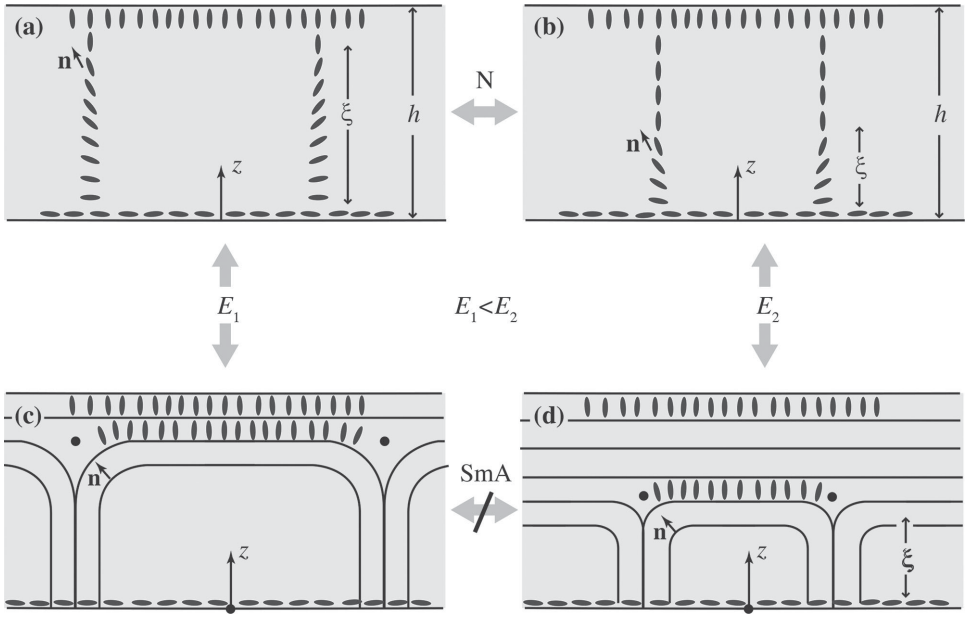

Figure 7. Internal structure of a linear domain in the presence of an electric field E. In the N phase, the director **n** tilts from the surface normal z in a layer with thickness comparable to the coherence length $\xi \propto 1/E$. The height of the LD in the SmA is comparable to ξ. Varying E is not sufficient to change the size of the LDs due to the topological barrier preventing the creation, rearrangement and adsorption of the defects (black dots).

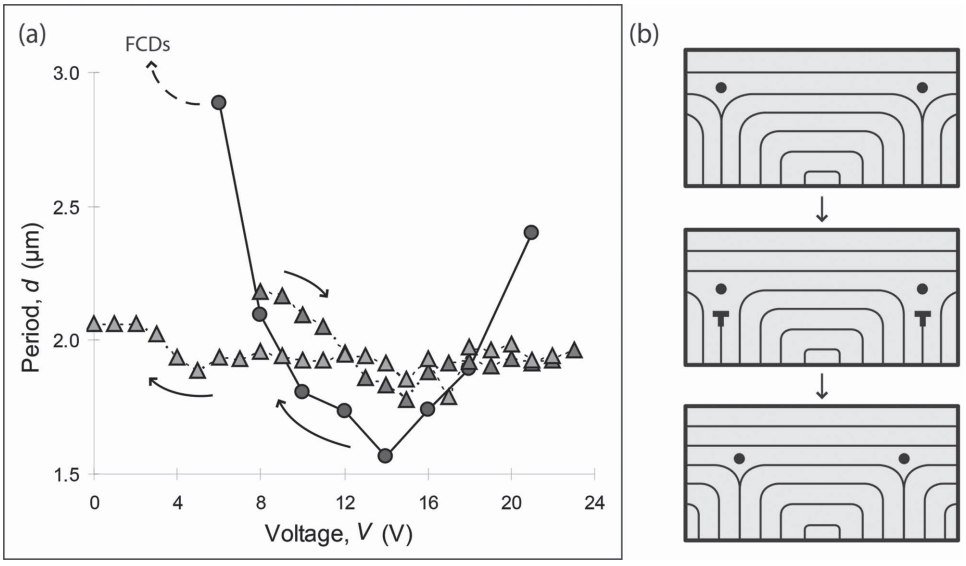

Figure 8. a) Persistence of the LD array period d as a function of the voltage V in the SmA phase. Dots correspond to arrays created by applying the voltage while cooling from the N to the SmA phase. In this case, d varied as a function of V and, for $V < 5$ V, 1d arrays were replaced by 2d lattices. Triangles correspond to an array created by applying 8V in the N phase. After the transition, the voltage was first increased (purple triangles) then decreased (green triangles) while keeping the sample in the SmA phase, without reheating in the N phase. In this case, d did not change with V and the 1d-2d transition was not observed. The sample thickness was $h = 11.7$ μm. b) Reducing the thickness of the region where lamellae are curved requires removing a curved lamella and creating dislocations (T symbols). Dots indicate disclinations lines and curvature walls.

explain the persistence of 1d patterns and their period when the field is decreased or switched off.

The likely cause of the pattern bistability and persistence is that rearranging the lamellae in response to variations of the confinement thickness (h when $E = 0$ or ξ when $E > 0$) involves large energy barriers: Our samples remained locked or 'frozen' in a non-equilibrium state at the N-SmA transition, when the constraints of the SmA phase were activated. Indeed, the study of striped patterns and two-dimensional (translation-invariant) periodic materials, particularly liquid crystals[44,45] and cylindrical bloc copolymers,[44,46,47] has shown that pattern kinetics is dominated by the large energy barriers required to change the number, type and relative distances of topological defects. Namely, the conservation of the total Burger's vector acts as a global constraint during pattern transformation. Defects also affect the macroscale rheology of SmA LC phases and generate bistability in SmA displays.[48] Figure 8b schematically shows the progressive confinement of a 1d array of LDs due to an increasing electric field. As ξ is reduced, a stack of horizontal layers grows from the surface inducing homeotropic anchoring and curved lamellae must be progressively removed from the flattened hemicylinder. Layer removal involves the creation of dislocations, an energy-costly process that requires violation of the constant-period constraint (confocality rule) around the dislocation core.

3. Conclusions

Applying electric fields is a simple and effective way to guide the nucleation of defects in SmA films and their self-assembly into periodic micropatterns. Compared to other methods such as microchannel confinement[20] or surface patterning,[49] applying electric fields gives the advantage of reconfigurability and bistability that are sought for optical applications[26,48,50] and may be beneficial in many applications such as guided assembly of nanoparticles interacting with defects[14] and fabrication of microlens arrays.[26] Moreover, 1d arrays with periods smaller than 1 μm can be easily created by applying electric fields to thick cells, instead of fabricating sub-micrometer cells without field. From the fundamental point of view, the smectic order in 1d array has the property of being translation-invariant (along y, Figure 4a) and can be studied using the methods developed for two-dimensional periodic systems such as block copolymers,[44,46] natural patterns, wavelets and wrinkles[51,52] and smectic phases of superconducting materials.[53] Also, our work with closed cells and electric fields evidences the generality – yet to be explained theoretically – of the confinement-induced 2d to1d transition for a decreasing confinement thickness, previously reported for open films of 8CB on various substrates (molybdenite,[12] mica[13] and poly-vinyl alcohol[14]). This phenomenon is largely independent on the confinement type (sample thickness h or coherence length ξ), interface chemistry (8CB or SCE12 at various substrates), boundary rigidity (glass plates vs air interface), surface anchoring strength, pre-tilt and order (smooth crystalline vs rough amorphous polymer substrates), as long as the surfaces induce conflicting homeotropic and unidirectional planar anchoring.

4. Experimental Details

LC Materials: 8CB (4′-octyl-4-biphenylcarbonitrile from Sigma-Aldrich) has the phase sequence SmA ↔ 32.5 °C ↔ N ↔ 40 °C ↔ Isotropic. SCE-12 (from Merck, England) is a ferroelectric mixture with negative dielectric constant, showing the sequence SmC* ↔ 64 °C SmA ↔ 78.8 °C ↔ N* ↔ 118.0 °C ↔ Isotropic, where * indicates chiral

phases.[54] SCE-12 molecules contain phenyl and biphenyl cores linked together by carbonyl bonds.

Substrates and Anchoring: We used glass plates as cell boundaries, with a thickness of 1 mm, covered with 100 nm thick, optically transparent and electrically conductive layer indium-tin-oxide (ITO). Homeotropic anchoring was obtained by dipping the glass for 20 minutes in a 90/10 w/w solution of *n*-hexane/chloroform containing 2.5 mM of octadecyl-trichloro-silane (OTS, from Sigma Aldrich), followed by drying at 110 °C for 1 h. Planar anchoring was obtained by rubbing a poly imide layer (PI-2555, from Hitachi Chemical DuPont MicroSystems GmbH) with thickness around 100 nm deposited on glass by spin-coating a 1/20 w/w solution of PI and *N*-methyl-2-pyrrolidone (NMP). The layer was baked at 80 °C for 30 min and at 250 °C for about 1 h to cross-link the PI polymer chains.

Optical Characterization: The local sample thickness h was determined for empty cells using an optical interferometry scheme that combined a microscope with a spectrophotometer (AvaSpec by Avantes). Light transmitted under normal incidence was modulated by multiple reflections at the partially reflecting glass boundaries, producing maxima of intensity at wavelengths λ_q such that $2\pi h/\lambda_q = hk_q = \pi q + \phi_{OTS} + \phi_{PI}$, where q is the chromatic order, k is the wave vector, and ϕ is the phase shift upon reflection at the air/OTS and air/PI interface. The intensity is a periodic function of $k = 2\pi/\lambda$ and we determined h by measuring the period $k_q - k_{q-1} = \pi/h$. To determine the lateral width d of a domain we used a polarized optical microscope (POM) with a 20× magnification. The phase retardation $\Gamma = h\delta n$ of linear domains was measured on the region of maximum birefringence δn using a Berek tilt compensator (Leica). The birefringence $\delta n = n^* - n_o$ is given by:

$$n^* = (1/h)\int_0^h [(\sin\theta(z)/n_e)^2 + (\cos\theta(z)/n_o)^2]^{-1/2}\, dz \qquad (1)$$

where θ is z-dependent angle of tilt between the director and the surface normal z. n_o and n_e are respectively the ordinary and extraordinary refractive indices of LC. $\Gamma/h = 0$ and $\Gamma/h = n_e - n_o$ when $\theta = 0$ and $\theta = 90°$, respectively.

Supporting Information

Supporting Information is available from the Wiley Online Library or from the author.

Acknowledgements

The authors thank Dr. Pasquale Pagliusi at the University of Calabria for kindly providing the OTS. The authors also thank J. C. Loudet and P. Cluzeau for providing SCE12.

Received: August 21, 2014
Revised: October 4, 2014
Published online: November 6, 2014

[1] A. M. Urbas, M. Maldovan, P. DeRege, E. L. Thomas, *Adv. Mater.* **2002**, *14*, 1850.
[2] C. Park, J. Yoon, E. L. Thomas, *Polymer* **2003**, *44*, 6725.
[3] M. P. Stoykovich, H. Kang, K. C. Daoulas, G. Liu, C. C. Liu, J. J. de Pablo, M. Mueller, P. F. Nealey, *ACS Nano* **2007**, *1*, 168.
[4] M. Mitov, C. Portet, C. Bourgerette, E. Snoeck, M. Verelst, *Nat. Mater.* **2002**, *1*, 229.
[5] H. K. Bisoyi, S. Kumar, *Chem. Soc. Rev.* **2011**, *40*, 306.
[6] Y. H. Kim, D. K. Yoon, H. S. Jeong, O. D. Lavrentovich, H. T. Jung, *Adv. Funct. Mater.* **2011**, *21*, 610.
[7] J. P. F. Lagerwall, G. Scalia, *Curr. Appl. Phys.* **2012**, *12*, 1387.
[8] J. S. Lintuvuori, A. C. Pawsey, K. Stratford, M. E. Cates, P. S. Clegg, D. Marenduzzo, *Phys. Rev. Lett.* **2013**, *110*, 187801.
[9] J. S. Pendery, O. Merchiers, D. Coursault, J. Grand, H. Ayeb, R. Greget, B. Donnio, J. L. Gallani, C. Rosenblatt, N. Felidj, Y. Borensztein, E. Lacaze, *Soft Matter* **2013**, *9*, 9366.
[10] R. S. Zola, L. R. Evangelista, Y. C. Yang, D. K. Yang, *Phys. Rev. Lett.* **2013**, *110*.
[11] P. T. Mather, *Nat. Mater.* **2007**, *6*, 93.
[12] J. P. Michel, E. Lacaze, M. Alba, M. de Boissieu, M. Gailhanou, M. Goldmann, *Phys. Rev. E* **2004**, *70*, 011709.
[13] B. Zappone, E. Lacaze, *Phys. Rev. E* **2008**, *78*, 061704.
[14] D. Coursault, J. Grand, B. Zappone, H. Ayeb, G. Levi, N. Felidj, E. Lacaze, *Adv. Mater.* **2012**, *24*, 1461.
[15] J. Milette, S. J. Cowling, V. Toader, C. Lavigne, I. M. Saez, R. B. Lennox, J. W. Goodby, L. Reven, *Soft Matter* **2012**, *8*, 173.
[16] G. Friedel, *Ann. Phys.* **1922**, *18*, 273.
[17] J. B. Fournier, G. Durand, *J. Phys. II* **1991**, *1*, 845.
[18] C. Blanc, M. Kleman, *Eur. Phys. J. E* **2001**, *4*, 241.
[19] L. Z. Ruan, J. R. Sambles, I. W. Stewart, *Phys. Rev. Lett.* **2003**, *91*, 033901.
[20] M. C. Choi, T. Pfohl, Z. Y. Wen, Y. Li, M. W. Kim, J. N. Israelachvili, C. R. Safinya, *Proc. Natl. Acad. Sci. USA* **2004**, *101*, 17340.
[21] B. Zappone, C. Meyer, L. Bruno, E. Lacaze, *Soft Matter* **2012**, *8*, 4318.
[22] A. Honglawan, D. A. Beller, M. Cavallaro, R. D. Kamien, K. J. Stebe, S. Yang, *Proc. Natl. Acad. Sci. USA* **2013**, *110*, 34.
[23] C. Blanc, D. Coursault, E. Lacaze, *Liq. Cryst. Rev.* **2013**, *1*, 83.
[24] D. K. Yoon, M. C. Choi, Y. H. Kim, M. W. Kim, O. D. Lavrentovich, H. T. Jung, *Nat. Mater.* **2007**, *6*, 866.
[25] Y. H. Kim, D. K. Yoon, H. S. Jeong, H. T. Jung, *Soft Matter* **2010**, *6*, 1426.
[26] Y. H. Kim, H. S. Jeong, J. H. Kim, E. K. Yoon, D. K. Yoon, H.-T. Jung, *J. Mater. Chem.* **2010**, *20*, 6557.
[27] P. G. De Gennes, J. Prost, *The Physics of Liquid Crystals*, Oxford **1974**.
[28] M. Kléman, *Points, Lines and Walls in Liquid Crystals, Magnetic Systems and Various Ordered Systems*, Wiley, New York **1983**.
[29] J. B. Fournier, *Phys. Rev. Lett.* **1993**, *70*, 1445.
[30] G. P. Alexander, B. G.-g. Chen, E. A. Matsumoto, R. D. Kamien, *Phys. Rev. Lett.* **2010**, *104*, 257802.
[31] E. Lacaze, J. P. Michel, M. Alba, M. Goldmann, *Phys. Rev. E* **2007**, *76*, 041702.
[32] W. Guo, C. Bahr, *Phys. Rev. E* **2009**, *79*, 061701.
[33] B. Zappone, E. Lacaze, H. Hayeb, M. Goldmann, N. Boudet, P. Barois, M. Alba, *Soft Matter* **2011**, *7*, 1161.
[34] P. E. Cladis, S. Torza, *J. Appl. Phys.* **1975**, *46*, 584.
[35] B. Jerome, Y. R. Shen, *Phys. Rev. E* **1993**, *48*, 4556.
[36] R. Horn, *J. Phys.* **1978**, *39*, 105.
[37] J. P. Michel, E. Lacaze, M. Goldmann, M. Gailhanou, M. de Boissieu, M. Alba, *Phys. Rev. Lett.* **2006**, *96*, 027803.
[38] O. P. Pishnyak, Y. A. Nastishin, O. D. Lavrentovich, *Phys. Rev. Lett.* **2004**, *93*, 159801.
[39] M. J. Bradshaw, E. P. Raynes, J. D. Bunning, T. E. Faber, *J. Phys.* **1985**, *46*, 1513.
[40] L. M. Blinov, V. G. Chigrinov, *Electrooptic Effects in Liquid Crystal Materials*, Springer-Verlag, New York **1996**.
[41] G. Barbero, M. Meuti, *J. Phys.* **1986**, *47*, 341.
[42] A. Mazzulla, F. Ciuchi, J. R. Sambles, *Phys. Rev. E* **2001**, *64*.
[43] N. A. Clark, *Phys. Rev. Lett.* **1985**, *55*, 292.
[44] N. M. Abukhdeir, A. D. Rey, *New J. Phys.* **2008**, *10*, 063025.
[45] C. Liu, M. Muthukumar, *J. Chem. Phys.* **1997**, *106*, 7822.
[46] C. Harrison, D. H. Adamson, Z. D. Cheng, J. M. Sebastian, S. Sethuraman, D. A. Huse, R. A. Register, P. M. Chaikin, *Science* **2000**, *290*, 1558.
[47] C. Harrison, Z. D. Cheng, S. Sethuraman, D. A. Huse, P. M. Chaikin, D. A. Vega, J. M. Sebastian, R. A. Register, D. H. Adamson, *Phys. Rev. E* **2002**, *66*.

[48] D. Coates, in *Handbook of Liquid Crystals*, Vol. 2A (Eds: D. Demus, J. Goodby, G. W. Gray, H.-W. Spiess, V. Vill), Wiley-VCH, Weinheim **1998**.
[49] W. Guo, S. Herminghaus, C. Bahr, *Langmuir* **2008**, *24*, 8174.
[50] C. Jones, in *Handbook of Visual Display Technology*, (Eds: J. Chen, W. Cranton, M. Fihn), Springer/Canopus, Bristol, UK **2012**.
[51] C. Bowmann, A. C. Newell, *Rev. Mod. Phys.* **1998**, *70*, 289.
[52] B. Li, Y. P. Cao, X. Q. Feng, H. J. Gao, *Soft Matter* **2012**, *8*, 5728.
[53] A. Mesaros, K. Fujita, H. Eisaki, S. Uchida, J. C. Davis, S. Sachdev, J. Zaanen, M. J. Lawler, E. A. Kim, *Science* **2011**, *333*, 426.
[54] J. C. Loudet, P. V. Dolganov, P. Patricio, H. Saadaoui, P. Cluzeau, *Phys. Rev. Lett.* **2011**, *106*, 117802.